Published in final edited form as:
Mol Cancer Ther. 2009 March ; 8(3): 499–508. doi:10.1158/1535-7163.MCT-08-0544.

Inhibition of Vimentin or β1-integrin Reverts Morphology of Prostate Tumor Cells Grown in Laminin-rich ECM gels and Reduces Tumor Growth *in vivo*

Xueping Zhang[1,*], **Marcia V. Fournier**[2,*], **Joy L. Ware**[3], **Mina J. Bissell**[2], **Adly Jacoub**[4], and **Zendra E. Zehner**[1]

1*Department of Biochemistry and Molecular Biology, Massey Cancer Center, Virginia Commonwealth University-Medical Campus, Richmond VA 23298*

2*Life Sciences Division, Lawrence Berkeley National Laboratory, Berkeley, CA 94720*

3*Department of Pathology, Massey Cancer Center, Virginia Commonwealth University-Medical Campus, Richmond VA 23298*

4*Department of Radiation Oncology, Massey Cancer Center, Virginia Commonwealth University-Medical Campus, Richmond VA 23298*

Abstract

Prostate epithelial cells grown embedded in laminin-rich extracellular matrix (lrECM) undergo morphological changes that closely resemble their architecture *in vivo*. In this study, growth characteristics of three human prostate epithelial sublines derived from the same cellular lineage, but displaying different tumorigenic and metastatic properties *in vivo*, were assessed in three-dimensional (3D) lrECM gels. M12, a highly tumorigenic and metastatic subline, was derived from the immortalized, prostate epithelial P69 cell line by selection in athymic, nude mice and found to contain a deletion of 19p-q13.1. The stable re-introduction of an intact human chromosome 19 into M12 resulted in a poorly tumorigenic subline, designated F6. When embedded in lrECM gels, the parental, non-tumorigenic P69 line produced acini with clearly defined lumena. Immunostaining with antibodies to β-catenin, E-cadherin, or α6- and β1-integrins showed polarization typical of glandular epithelium. In contrast, the metastatic M12 subline produced highly disorganized cells with no evidence of polarization. The F6 subline reverted to acini-like structures exhibiting basal polarity marked with integrins. Reducing either vimentin levels via siRNA interference or the expression of α6-, β1-integrins by the addition of blocking antibodies, reorganized the M12 subline into forming polarized acini. The loss of vimentin significantly reduced M12-Vim tumor growth when assessed by subcutaneous injection in athymic mice. Thus, tumorigenicity *in vivo* correlated with disorganized growth in 3D lrECM gels. These studies suggest that the levels of vimentin and β1-integrin play a key role in the homeostasis of the normal acinus in prostate and that their dysregulation may lead to tumorigenesis.

Keywords

prostate; 3D culture; tumor progression; vimentin; α6β1-integrin; lrECM

2. Corresponding Author: Zendra E. Zehner, P.O. Box 980614, Department of Biochemistry and Molecular Biology, Virginia Commonwealth University, Richmond, VA 23298-0614. Phone: 804-828-8753; Fax: 804-828-1473. E-mail: E-mail: zezehner@vcu.edu.
X. Zhang and M. Fournier contributed equally to this work.

3. No Conflict of Interest

Introduction

The extracellular environment is essential for establishing and maintaining cell differentiation during glandular morphogenesis (1). In the developing prostate, budding urogenital epithelial cells attach to the extracellular matrix (ECM) through integrin receptors and migrate into the mesenchyme to form acini containing lumen and displaying polarity (2). Integrins play an important role in maintaining the bi-directional communication between prostate cells and the ECM. Moreover, their expression patterns are known to change during tumor progression; for example, β1-integrin levels increase whereas β2 and β3 remain unchanged (3). Differential expression of α6- and α3-integrins suggests a reorganization of adhesion complexes during prostate cancer progression (4). Since α6β1-integrin is one leading component of these complexes, it was proposed that inhibition of either α6- or β1-integrin might reverse the invasive phenotype (5). Tumor stromal interactions have also been found to influence prostate cancer progression (6). Abnormal stroma containing cancer-associated fibroblasts promoted carcinogenesis of non-tumorigenic, genetically abnormal epithelial cells, but had no effect on normal epithelial cells. Growth of cells in three-dimensional (3D) environments, which better mimic the normal cellular microenvironment, offer unique approaches for elucidating signals that contribute to tumor progression *in vivo* (7).

Prostate tumors display a loss of the epithelial marker E-cadherin and a switch in intermediate filament protein (IFP) expression from keratins to vimentin, resulting in the loss of hemidesmosomes (5). This switch in expression may earmark cells that have undergone an epithelial to mesenchymal transition (EMT). In cancer, the EMT may be a step towards tumor invasion, although this hypothesis remains controversial (8–10). Nonetheless, a role for vimentin in motility has been well documented in several cell types and may be important in cancer where motility is one component required to establishing a metastatic phenotype. Motility and migration of breast, head and neck, or colon cancer cells was markedly affected by vimentin RNAi (11–14). Although extensive studies are lacking in prostate, the expression of vimentin may be an underappreciated component of prostate tumor growth and progression.

Normal methods for culturing cells on plastic tissue culture dishes, referred to as two dimensional (2D), do not duplicate the natural milieu surrounding epithelial cells *in vivo* nor do they produce polarized acini surrounded by basement membrane, as found in normal prostate tissue (15). To alleviate this problem, epithelial cells have been cultured in 3D in laminin-rich ECM gels (lrECM) (16). Since cells grown in lrECM gels closely duplicate glandular phenotypic characteristics, these cultures enable an investigation into the influence of ECM and stroma on cell growth and differentiation *in vitro* (5,16,17). In the case of prostate epithelial, a variety of different morphological structures have been obtained depending on cell type and culture conditions. For example, RWPE-1, an immortalized, non-tumorigenic prostate epithelial cell line, was able to migrate into- and form branches terminating in- acini when plated on top of lrECM gels (2). However, NMU-transformed RWPE-1 cells formed solid cell masses (18). Cultures of RWPE-2, a Ki-ras transformed subline of RWPE-1, resulted in single to small clumps of cells with no evidence of acinus organization. The unrelated human prostatic carcinoma cell lines DU-145, PC3 or PNTC-C2 formed amorphous balls called spheroids without organization or lumen (2,19). These different results could be due to the comparison of genetically dissimilar cell lines or related sublines, which were plated on top of lrECM gels rather than embedded. Due to these inconsistent results, we initiated a more thorough analysis of the morphological structures formed by a unique set of genetically related, malignant or non-malignant prostate sublines grown embedded in lrECM gels.

P69 is an immortalized, non-metastatic prostate epithelial cell line (20). A metastatic subline M12 was derived by *in vivo* selection (3 passages) of P69 cells in male, athymic nude mice (21). Analysis of M12 chromosomal alterations detected a novel 16:19 unbalanced

translocation resulting in the deletion of one copy of 19p-q13.1. Microcell-mediated chromosome transfer restored an intact, neomycin-marked human chromosome 19 (Chr19) to generate the F6 subline (22). The M12 subline is fast growing and highly metastatic upon orthotopic injection in athymic, nude mice whereas the F6 subline is slow growing, barely forms small tumors, and is not metastatic. These related sublines present an excellent model for investigating requirements for prostate cancer tumor progression.

The behavior of the P69, M12 and F6 human prostate epithelial sublines was analyzed in 3D cultures and compared to the LNCaP and PC3 cell lines. Under these conditions, we found distinct differences in their morphological properties, which correlated with their behavior *in vivo*. The addition of blocking antibodies to α6 or β1-integrin, or the stable repression of vimentin expression via shRNA technologies enabled the highly tumorigenic, metastatic M12 cells to form organized acini structures akin to those formed by the P69, F6 sublines.

Materials and Methods

Substrates and antibodies

Commercially prepared EHS extracellular matrix extract, growth-factor reduced, lrECM (Cultrex BME) was used for 3D cultures (23). Antibodies used for Western blotting and immunostaining studies were as follows: androgen receptor (AR sc-7305: Santa Cruz Biotech., Santa Cruz, CA), E-cadherin (U3254: Sigma, St. Louis, MO), β-catenin (H-102: Santa Cruz Biotech.), keratin 5/6 (Dako NA Inc., Carpinteria, CA), keratin 8 (ab9287; Abcam, Cambridge, MA), β1-integrin (MAB1951Z: Chemicon, Temecula, CA), α6-integrin (MAB1378: Chemicon), Ki-67 (clone MIB: Jackson ImmunResearch Labs., West Grove, PA), vimentin (V6630: Sigma) and β–actin (A5441: Sigma). FITC-conjugated anti-rat IgG was from Jackson IR Laboratories whereas fluorescent Alexa488/546-labeled anti-rabbit and mouse IgG were from Invitrogen (Carlsbad, CA). Blocking antibodies for β1-integrin (AIIB2) originally a gift from C. Damsky was isolated and prepared from a hybridoma cell line (Sierra Biosources, Milipitas, CA) whereas α6-integrin blocking antibody (GoH3) was from BDPharmingen. Nonspecific rat and mouse IgG and HRP-conjugated secondary antibodies were from Santa Cruz Biotech. Goat $F(ab')^2$ anti-mouse IgG was from Invitrogen (MAB35000).

Cell culture and stable transfectants

The establishment, maintenance and characterization of the SV40 T antigen-immortalized human prostate epithelial cell sublines, P69, M12, and F6 have been previously described (21,22,24). M12 cells were stably transfected with a plasmid psiREN+RetroQ (BD Biosciences, San Jose, CA) expressing a human vimentin shRNA (M12-Vim) of sequence 5'-GATCCGCACCGAGTTCAAGAACACCTTTTCAAGAGA-GGTGTTCTTGAACTCGGTGTTCTTTTTTTTCTAGAG-3' [the human vimentin gene sequence is underlined] as previously described (14). M12 cells transfected with either the empty pSiREN+RetroQ vector (M12+siREN) or vector containing a non-targeting control sequence (M12+NTC: 5'-GATCCGGCATGTACTAGCCTAAGCGTTTTCAAGA-GACGCTTAGGCTAGTACATGC-TTCTTTTTTTCTAGAG-3') served as negative controls. A search of the human genome or Sanger microRNA database confirmed no significant match to the non-targeting control sequence. Cells were transfected using *Trans*IT-LT1 transfection reagent (Mirus Bio Corp., Madison, WI) according to manufacturer's instructions. Puromycin-resistant cells were selected in 400 ng/ml of puromycin and maintained in 100 ng/ml (Amersham Biosciences, Piscataway, NJ). The down-regulation of vimentin gene expression in stable transformants designated as M12-Vim was confirmed by Western blot analysis. LNCaP cells were cultured in RPMI-1640 media plus 10% FBS and 1% pen/strep (25). PC3 cells were retrieved from tumors grown in athymic mice and maintained in RPMI-1640 for 5 passages before embedding in lrECM as previously described (25).

Acinar morphogenesis

3D cultures were prepared by growing prostate cancer cells to 80% confluence of monolayer on plastic tissue culture dishes, followed by trypsinization and collection by centrifugation. LrECM was pre-thawed on ice overnight. Cells (1×10^6) were mixed with 1 ml of undiluted lrECM and added to each well of a 6-well dish. Following incubation for 1 hr at 37°C, the lrECM had polymerized. Medium (3 ml) containing a specific drug, if needed as cited above, was added on top of the solidified lrECM-cell mix. The same batch of lrECM was used throughout this study. Medium was replaced every other day and cultures grown for up to 16 days in lrECM, maintaining their organization for this entire period.

In vivo tumorigenicity assays

Tumorigenicity of M12 cells stably transformed with the vimentin shRNA expression plasmid (M12-Vim), vector alone (M12+siREN), or vector expressing the non-targeting RNA control (M12+NTC), was assessed by subcutaneous injection of 1×10^6 cells into male, athymic nude mice as described previously (21). A total of 15 mice were injected as follows: 6 mice with M12-Vim, 4 mice with M11+siREN and 5 mice with M12+NTC for a total of 9 mice serving as negative controls. Tumor growth was monitored by caliper measurement for up to 42 days and approximate tumor volume (mm^3) was calculated as length × $width^2/2$. At the time of euthanasia, tumors were removed, samples fixed in 10% buffered formalin, paraffin-embedded, stained, and examined for vimentin expression. All experiments were conducted under a protocol approved by the Institution Animal Care and Use Committee of Virginia Commonwealth University.

Western immunoblotting

Harvested cells were washed with cold 1×PBS and then lysed in 4% SDS in 1×PBS with protease inhibitor cocktail (Sigma). After brief sonication, an equal volume of 1×PBS was added to reduce the SDS concentration to 2%. Lysates were then centrifuged for 10 min at high speed, supernatants collected, and protein concentration measured using the BioRad D_c Protein Assay kit (BioRad, Hercules, CA). Equivalent amounts of protein (40 μg) were boiled in 1×SDS sample buffer for 5 min and analyzed on 8–16% gradient polyacrylamide gels (NuSep Inc., Austell, GA). Western immunoblot analysis was performed and quantified as previously described (26).

Morphological structures from the various P69 derived cells grown in lrECM gels were harvested as described (23). Cells were transferred to a 50 ml centrifuge tube with 10 ml of 0.5% Na_2EDTA in 1×PBS plus 1% protease inhibitor cocktail. The mixture was shaken on ice for 1 hr to completely dissolve the lrECM gel, after which cells were collected at 1,000 rpm for 5 min, washed twice with 1×PBS plus protease inhibitor cocktail and stored at −80°C. Cell extracts were prepared and Western immunoblot analysis performed as previously described (26).

Indirect immunofluorescence

A sample (≅10 μl) of lrECM culture was spread on each well of a 4-well chamber slide, air dried, and fixed in 1:1 methanol-acetone at −20°C for 10 min. The slides were washed by 1×PBS briefly, followed by 400 μl 1×IF buffer (130mM NaCl, 7mM Na_2HPO_4, 3.5mM NaH_2PO_4, 7.7mM NaN_3, 0.1% bovine serum albumin, 0.2% Triton X-100, 0.05% Tween-20) with 10% goat serum and a secondary blocking in 200 μl 1×IF buffer with 10% goat serum and 20 μg/ml goat anti-mouse $F(ab')_2$ fragment for 1 hr sequentially. Slides were incubated with primary antibody overnight at 4°C followed directly by either FITC or Alexa-conjugated secondary antibody (1:200) for 45 min. The dilution of antibodies used were as follows: α6-integrin (1:100), AR (1:50), β-catenin (1:100–200), β1-integrin (1:100), keratin 5/6 (1:200),

keratin 8 (1:100), E-cadherin (1:200), vimentin (1:200), and Ki-67 (1:200). Nuclei were counterstained with di-amino-phenyl-indole (DAPI, Sigma) overnight at room temperature. Control slides were stained with secondary antibody only. Slides were visualized under a LZM5100 confocal microscope according to the manufacturer's instructions. Representative pictures were shown from experiments repeated at least twice with 20–50 morphological structures analyzed.

Reversion assay

Equal densities of cells were seeded in lrECM gels containing AIIB2 (160 μg/ml), GoH3 (5 μg/ml), DMSO only or IgG (5 μg/ml) as negative controls. After 10 days, cells were photographed and stained with specific antibodies as discussed above.

Statistical Analyses

Data are presented as the mean ± the standard error (S.E.). A regression model was performed to validate significant differences. Statistical analysis used JMP statistical software (Cary, NC) with significance set at a probability of ≤ 0.05. Where indicated immunofluorescence staining was quantitated using image J software (NIH). For example, in compiling date for Table 1 an average value was generated from the quantification of 4 arbitrary sections of each morphological structure shown in Fig. 2 and compared across panels (panel d_1 through d_4) to generate an arbitrary scale of +++ to −.

Results

Morphological properties of P69, M12 and F6 sublines grown embedded in lrECM gels

When grown on plastic tissue culture dishes (2D), the cellular morphology of the P69 derived prostate cell sublines is indistinguishable (Fig. 1A, top row). However, when grown embedded (3D) in lrECM gels, these genetically similar sublines organize into distinct, different morphological structures (Fig. 1A, bottom row and Fig. 2). The non-tumorigenic P69 epithelial cell line forms acini (Fig. 1A, lane 1). Although the highly metastatic M12 subline initially forms solid balls of cells called spheroids, within 48 hrs the cells began to migrate out of these structures and ultimately penetrate throughout the lrECM gel (Fig. 1A, lane 2). The poorly tumorigenic F6 subline reverted back to forming acini (Fig. 1A, lane 3).

A proteomic analysis of these sublines revealed a notable difference in the expression of the mesenchymal IFP, vimentin (24). Epithelial cells grown on plastic dishes often aberrantly express vimentin (Fig. 1B, top row) albeit at a low level compared to the usual epithelial keratins (27). When grown in 3D, vimentin is not expressed in the P69 subline, akin to expression patterns *in vivo* (Fig. 1B, bottom row). Similar to most, if not all metastatic cancers, vimentin is highly expressed in the metastatic M12 subline grown either in 2D or 3D (28). Conversely, the amount of vimentin protein is severely reduced in the F6 subline grown under either condition (24). Thus, in both cases, the M12 subline highly expresses vimentin, while the P69 and F6 sublines either do not, or exhibit a marked decrease in vimentin expression when grown in lrECM gels.

Blocking vimentin via shRNA interference causes a dramatic change in the *in vitro* phenotype of M12 cells

Previous studies of non-isogenic breast cancer cell lines suggested that vimentin expression is essential, but not sufficient to cause tumor metastasis (29). In these prostate sublines there is a tremendous difference in vimentin expression (24). To determine if vimentin content could have a direct effect on the morphology of the M12 subline, M12s were stably transformed with a vimentin shRNA producing plasmid referred to as M12-Vim. When grown in either 2D or

3D the level of vimentin protein was repressed 85% compared to the wild-type M12 (Fig. 1B). When grown in 2D, there was no apparent difference between the morphology of the M12 versus M12-Vim sublines (Fig. 1A, top row). However, when grown in 3D the M12-Vim subline reverted to acini-like structures (Fig. 1B, bottom row).

Phenotypic characteristics of P69, M12, F6 and M12-Vim Grown in lrECM

The parental P69 subline forms smooth, regular acini when grown in lrECM gels (Fig. 2A). Confocal microscopy of a series of pictures taken at a fixed plane through an acinus (Z-stack) and immunostained with α6-integrin confirms the multicellular nature of these acini with a notable, clear lumen. The similarity of these structures to those formed by prostate glandular epithelium embedded in a matrix of stromal cells was readily apparent (2).

Immunostaining for a variety of relevant IFPs, nuclear, membrane and cell-surface proteins was used to access protein organization within the morphological structures formed by these sublines in lrECM gels (Figs. 2B and 2C). Staining for Ki-67 revealed that nuclei were actively dividing at day 8 for all sublines (Fig. 2B, panels a_1–a_4). P69 acini did not express vimentin (Fig. 2B, panel a_1), but did contain β-catenin (panel b_1), E-cadherin (panel c_1), keratin 5/6 (panel d_1), keratin 8 (panel e_1), and α6β1-integrin (Fig. 2C, panels h_1 and j_1) akin to normal prostate epithelial cells. The overlay (Fig. 2C, panel k_1) indicated that α6β1-integrin was co-localized and polarized on the outside edge of the acinus as seen in prostate tissue (5,30). In contrast, by day 8 most of the metastatic M12 subline had grown out of spheroids (Fig. 2B, panels a_2 to e_2 and 2C, panels h_2 and j_2). β-catenin staining of cell:cell junctions confirmed that these cellular masses were not organized into lumen-containing acini (Fig. 2B, panel b_2). In addition, there was a loss of expression (≅ 99%) of the epithelial cell marker, E-cadherin (panel c_2) co-incident with the emergence of vimentin (panel a_2) as seen in Fig. 1B. Moreover, the M12 cellular mass showed little organization and a loss of polarization as verified by diffuse staining with antibodies to α6- and β1-integrins (Fig. 2C, panels h_2 to k_2). In addition, expression of keratin 5/6 was barely detectable (Fig. 2B, panel d_2), whereas keratin 8 (panel e_2) remained consistent. In a time course study, it was evident that the M12 subline did initially try to form spheroids (a remnant of one is seen in Fig. 2B, panel a_2 , white arrow), but by day 8 most cells had migrated out of spheroids into the surrounding matrix.

Interestingly, F6 cells with a restored second copy of Chr 19 produced acini-like structures with a defined lumen (Figs. 2B and 2C). Expression of vimentin was greatly reduced (Fig. 2B, panel a_3) and expression of E-cadherin returned (panel c_3) as well as keratin 5/6 (panel d_3) with the multicellular nature of these acini confirmed by β-catenin staining of cell junctions (panel b_3). Keratin 8 (panel e_3) expression continued. Moreover, F6 acini exhibit α6 and β1-integrin polarization with co-localization (note overlay) of α6β1-integrin dimers (Fig. 2C, panels h_3 to k_3).

Reducing vimentin expression via shRNA also reverted M12 cells back to acini-like structures (Figs. 2B and 2C). Immunostaining with antibodies to vimentin and E-cadherin showed that the M12-Vim subline expressed E-cadherin and keratin 5/6 instead of vimentin (Fig. 2B, compare panels c_4 and d_4 to a_4). Western blots confirmed that P69, F6, or M12-Vim acini grown in lrECM gels (3D) retained E-cadherin expression whereas it was lost (99%) in the M12 subline (data not shown). Again, Keratin 8 (panel e_4) remained. M12-Vim cells exhibit polarization of α6- or β1-integrins and renewed co-localization of α6β1-integrin dimers (Fig. 2C, panels h_4 to k_4), which is similar to that seen in the P69 or F6 acini (Fig. 2C, panels k_1, and k_3). Since staining for AR was negative, both in Western blots of 2D cultures (31) and immunofluoresence staining of 3D structures, pictures are not shown.

Growth of these genetically-related sublines was compared to the more familiar prostate cell lines, LNCaP and PC3 (Fig. 2D). Only immunofluoresence staining for proteins relevant to

morphological organization are shown. Both cell lines formed multi-cellular spheroids with no evidence of a lumen upon Z-stack analysis. The least tumorigenic LNCaP's (AR+) displayed co-localization and polarization of α6β1-integrins akin to the F6 subline (overlay panel m_3). However, the highly metastatic PC3 cell line did not exhibit integrin polarization and staining was diffuse (overlay panel n_3) as in the M12 subline (Fig. 2C, panel k_2).

Measurement of P69, F6 and M12-Vim Acini Grown in lrECM

Next, we compared the growth properties of P69, F6 and M12-Vim structures overtime in 3D culture to determine if acini reach a maximum cell number, size, become growth arrested or maintain a lumen (Figure 3). Counting the number of nuclei in one hundred P69, F6 and M12-Vim acini indicated these cells were still actively dividing by day 13 in culture (Fig. 3A). Growth arrest occurred around day 16, as confirmed by negative staining for Ki-67 at day 16 compared to day 13 (data not shown). The size of the acini (um) also reached a maximal level by day 16, consistent with the cell number count per acinus (Fig. 3B). In contrast, M12 sublines still showed positive Ki-67 staining up to day 16. These cultures could not be analyzed past 16 days as the ability of the lrECM gel to support growth became rate limiting. Since M12 cells form a non-organized cellular mass rather than acini, it was not relevant to count nuclei. Data was analyzed by regression model with p-values of 0.15 and 0.08 (both>0.05) for cell number (Fig. 3A) and acini size (Fig. 3B), which indicates there is no significant difference between the 3 sublines.

Blocking vimentin expression in M12 cells affects tumor formation in nude, athymic mice

Previously, the tumorigenicity of the M12 and F6 subline was determined by subcutaneous injection into male, athymic, nude mice (21). All mice (13/13) injected with M12 cells developed tumors after 9–15 days. Mice injected with F6 cells either failed to produce tumors (9/15) or produced only small tumors (6/15) after 120 days. When grown in 3D, reducing the expression of vimentin reverted the M12 cells back to acini-like structures. Next, we asked if the dramatic morphological difference observed *in vitro* would correlate to tumor growth *in vivo*? To answer this question, tumor formation was assessed by subcutaneous injection into male, athymic, nude mice of M12 cells stably transformed with vector only (M12+siREN), vector expressing a non-targeting, scrambled RNA sequence (M12+NTC) or M12-Vim (Fig. 4A). By 42 days 6/6 mice injected with M12-Vim displayed tumors, which were over 8-fold reduced in size compared to the average of the 9 mice injected with either the M12+siREN or M12+NTC negative controls. Importantly, there was little difference in the proliferation rate of the M12-Vim subline compared to the negative control cells in 2D culture (data not shown). Thus, the lack of vimentin is not influencing cell growth rate *in vitro*. Regression model analyses using the LSmeans Tukey HSD test, indicated that there was a significant difference between M12+NTC or M12+siREN versus M12-Vim with p-values <0.001. At the completion of the experiment, animals were euthanized, tumors were removed, and continued vimentin expression in the M12+siREN negative control verified by immunofluoresence staining (Fig. 4B, right panel). Little vimentin could be detected in the small tumors formed by the M12-Vim subline (Fig. 4B, left panel) in agreement with Western blots (Fig. 1).

A comparison of the morphological properties of these cells *in vitro* and *in vivo* is compiled in Table 1. Tumorigenicity of the original M12 and F6 sublines was documented previously (22). Here, the reduction of vimentin expression in the M12-Vim cells reduced tumor growth compared to the M12 control cells. A reduction in expression of E-cadherin concomitant with activation of vimentin expression is indicative of cells that have progressed through the EMT (8). It would appear that this transition is occurring in these genetically-related sublines when grown embedded in lrECM gels. Co-expression of keratin 5/6 and kertain 8 plus p63 (data not shown) suggest parental P69 cells were derived from an intermediate cell, proposed to be the progenitor cell of prostate cancer (32) Moreover, the lack of keratin 5 expression in the highly

tumorigenic, metastatic, M12 subline is consistent with loss of keratin 5 expression in human prostate cancer metastases (33,34,35). Overall, these comparisons support the conclusion that the growth of these uniquely related prostate sublines in 3D culture closely parallels their properties *in vivo* and those of glandular epithelium as cells progress to tumor formation and ultimately metastatic prostate carcinoma.

Inhibiting α6 or β1-integrin activity can cause a phenotypic reversion

The inclusion of blocking antibodies for β1-integrin (AIIB2) or α6-integrin (GoH3) reverted the M12 cells back to smooth acini-like structures whereas IgG had little affect (Fig. 5A). Similar treatment of the F6 subline showed little difference, although there may be a slight reduction in acinus size. Immunostaining with the E-cadherin antibody showed that treatment with either AIIB2 or GoH3 restored some E-cadherin expression, resulting in some evidence of polarization akin to F6 acini structures (Fig. 5B, panels c_2 and c_4 compared to panels d_2 and d_4). Importantly, neither the AIIB2 nor GoH3 antibody had an effect on F6 acini formation. Thus, this affect appears to be specific to M12 cells. Western blots demonstrated that AIIB2 treatment did dramatically decrease β1-integrin expression (≅85%) in both the M12 and F6 sublines, whereas vimentin expression in the M12 subline or actin levels in either subline was not affected (Fig. 5C). These results differed from other studies, where acinar formation of normal prostate epithelium was practically obliterated by the addition of either α6- or β1-blocking antibodies (18), but does agree with the fact that β1-integrin is more associated with the formation of focal adhesion complexes involved with motility than stable hemidesmosomal attachment sites used more for the anchoring of cells. To our knowledge, this is the first time that the effect of α6-, β1-integrin function-blocking antibodies has been tested against metastatic prostate cells rather than normal prostate epithelial in 3D, a more relevant assay for determining how changes in protein expression contribute to tumor progression.

Discussion

The analysis of relevant marker proteins (E-cadherin, keratins, β-catenin, and α6-, β1-integrins) in these genetically-related, human prostate epithelial sublines grown in lrECM gels demonstrates that the relative distribution and proportion of cell surface integrins controls the structural homeostasis of these cells. The parental P69 cell line produces structures that are morphologically similar to human glandular prostate epithelial cells (2). α6- and β1-integrin expression is polarized in the P69, poorly tumorigenic F6 and M12-Vim acini, but polarization disappears in the disorganized mass of tumorigenic and metastatic M12 cells. The weakly tumorigenic LNCaP cell line displayed features of integrin polarization akin to P69, F6 or M12-Vim sublines, but the metastatic PC3 cell line formed solid spheroids of cells similar to initial M12 cultures. With time the M12 subline grew out of such disorganized spheroids, which may reflect its highly metastatic phenotype (22). Thus, a thorough analysis of these P69 derived sublines has revealed *in vitro* morphological properties, which correlate with their tumorigenic/metastatic behavior *in vivo* and to the more common LNCaP and PC3 prostate cell lines (21, 22). Overall, our results agree with those studies where an inverse relationship was found between acinar formation and malignancy (2,36).

Recently, a correlation between vimentin expression and the degree of metastasis was confirmed in another set of genetically related prostate cells lines (37). More importantly, we found vimentin expression to be a crucial component of the morphological changes observed by cells grown in 3D. Disorganized M12 cells containing vimentin did not form acini in lrECM gels, but moved out of spheroids and spread throughout the matrix with little evidence of any acini structure. On the other hand, the P69 and F6 sublines express little vimentin, but did form acini-like structure in lrECM gels. Blocking vimentin gene expression via shRNA reverted M12 cells to producing acini-like structures. These results imply that the lack of vimentin

protein is essential for formation of acini-like structures by these sublines *in vitro*. M12-Vim cells displayed a considerable reduction in tumor growth *in vivo*, consistent with those morphological differences displayed *in vitro*. Although several studies document a requirement for vimentin in motility and invasion assays *in vitro*, this is the first indication of such a dramatic effect on prostate tumor growth *in vivo* dependent upon the continued expression of vimentin, although a similar role has been noted in breast, and head and neck cancer cell lines (11–14, 38,39).

An increase in β1-integrin expression has been found in actual prostate tumor samples as well as in more de-differentiated tumor cells (3,30). Similar results have been reported for metastatic mammary gland epithelial cell lines, where reversion by an inhibitory α6- or β1-integrin antibody or its $F(ab')^2$ fragment led to the re-establishment of E-cadherin-β-catenin complexes (40). In our study the interruption of α6- or β1-integrin expression reversed the morphological phenotype of the metastatic M12 subline back to organized, polarized acini in 3D as proposed, but never proven experimentally (5). Although β1-integrin inhibitory antibodies were shown to block acini formation in a previous study, cells were plated on top of LrECM and had to first move into the gel to subsequently form acini, addressing a different experimental question than here (18). Our results suggest that α6- or β1-integrin blocking antibodies could represent a relevant therapy to combat prostate tumor progression as has been suggested for metastatic breast cancer (41).

It has been postulated that in motile cells vimentin is responsible for moving endocytosed β1-integrin from the rear of the cell to the leading edge under the control of PKC-ε (42). Upon inhibition of PKC-ε and loss of vimentin phosphorylation, integrins become trapped in endocytic vesicles and directional motility towards the ECM is severely attenuated. Other studies proposed that vimentin functions as a carrier to move cargo on microtubules using kinesin/dynein motors (43). Although vesicle movement on the IFP network itself has never been documented, inhibitors that collapse microtubules affect the IFP network, suggesting cross-talk (43). Since the IFP network is the only filament that completely traverses the cytoplasm, a role in signal transduction has been proposed (44). Until now the nature of the cargo carried by vimentin in non-neuronal cells was unknown. Based on our results and the literature, we propose that vimentin may contribute to moving β1-integrin to the leading edge to support motility in prostate carcinoma. Since α6-integrin expression also correlates with a more metastatic phenotype and α6-blocking antibodies reverted the morphology of the M12 subline, α6-integrin may also play a role in prostate invasion (5,30,45,46). Currently, we propose that vimentin:β1-integrin interaction is required for motility, an important precondition for establishing the metastatic property of M12 cells *in vivo*. Interrupting this movement by blocking α6, β1-integrin antibodies or reducing the amount of vimentin protein via shRNA interference reverted cells to acini-like structures *in vitro* and severely reduced growth in nude mice. We propose that by understanding the nature of the vimentin:integrin interaction, perhaps target molecule(s) could be generated to block this association. These molecules would be specific for the poorly differentiated, highly metastatic cell, since it is only this cell-type that is motile and highly expresses both α6, β1-integrin and vimentin (19,47). Such molecules may also present a relevant therapy for other poorly differentiated metastatic tumors such as breast, which also co-express β1-integrin and vimentin at high levels (28).

In summary, growth of the P69, M12 and F6 sublines in lrECM gels presents a biologically relevant model system for determining what controls morphological differences *in vitro* that contribute to promote tumor progression *in vivo*. It is anticipated that growth of these unique prostate sublines in 3D will lead to the detection of relevant markers/targets that could be useful in the diagnosis, prevention and ultimate treatment of prostate tumor progression. In addition, these sublines and the 3D technology could be easily adapted to high throughput screening for

drugs, which could modify M12 morphological behavior *in vitro*, and identify a useful future therapy to counteract high tumor growth rates and/or metastasis *in vivo*.

Abbreviations

AR, androgen receptor; AIIB2, monoclonal antibody to β1-integrin; Chr 19, chromosome 19; EMT, epithelial mesenchymal transition; GoH3, monoclonal antibody to α6-integrin; IFP, intermediate filament protein; lrECM, laminin-rich extracellular matrix; 3D, three dimensional.

Acknowledgements

1. Financial Support: Department of Defense grant DAMD 17-00-1-0296 and the Virginia Commonwealth Health Research Board 40-06 to Z.E. Zehner, and NCI grant 2 RO1 CA064786-09 and U.S. Department of Defense Breast Cancer Research Program Innovator Award grant BC012005 to M.J. Bissell.

We thank Ms. Frances K. White and the confocal imaging facility from the Massey Cancer Center supported in part by NIH Grant P30CA16059 and Dr. Davis Massey, Dept. of Pathology, VCU School of Medicine, for photography of immunofluoresence stained tissue.

References

1. Barcellos-Hoff MH, Aggeler J, Ram TG, Bissell MJ. Functional differentiation and alveolar morphogenesis of primary mammary cultures on reconstituted basement membrane. Development 1989;105:223–235. [PubMed: 2806122]
2. Webber MM, Bello D, Kleinman HK, Hoffman MP. Acinar differentiation by non-malignant immortalized human prostatic epithelial cells and its loss by malignant cells. Carcinogenesis 1997;18:1225–1231. [PubMed: 9214606]
3. Murant SJ, Handley J, Stower M, Reid N, Cussenot O, Maitland NJ. Co-ordinated changes in expression of cell adhesion molecules in prostate cancer. Eur J Cancer 1997;33:263–271. [PubMed: 9135498]
4. Schmelz M, Cress AE, Scott KM, et al. Different phenotypes in human prostate cancer: α6 or α3 integrin in cell-extracellular adhesion sites. Neoplasia 2002;4:243–254. [PubMed: 11988844]
5. Cress AE, Rabinovitz I, Zhu W, Nagle RB. The alpha6 beta1 and alpha6 beta4 integrins in human prostate cancer progression. Cancer Metastasis Rev 1995;14:219–228. [PubMed: 8548870]
6. Cunha GR, Hayward SW, Wang YZ, Ricke WA. Role of the stromal micro-environment in carcinogenesis of the prostate. Int J Cancer 2003;107:1–10. [PubMed: 12925950]
7. Bissell MJ, Rizki A, Mian IS. Tissue architecture: the ultimate regulator of breast epithelial function. Curr Opin Cell Biol 2003;15:753–762. [PubMed: 14644202]
8. Gilles C, Thompson EW. The epithelial to mesenchymal transition and metastatic progression in carcinoma. Breast J 1996;2:83–96.
9. Thompson EW, Newgreen DF, Tarin D. Carcinoma invasion and metastasis: A role for epithelial-mesenchymal transition? Cancer Res 2005;65:5991–5995. [PubMed: 16024595]
10. Tarin D, Thompson EW, Newgreen DF. The fallacy of epithelial mesenchymal transition in neoplasia. Cancer Res 2005;65:5996–6000. [PubMed: 16024596]
11. Hendrix MJ, Seftor EA, Chu YW, Trevor KT, Seftor RE. Role of intermediate filaments in migration, invasion and metastasis. Cancer Metastasis Rev 1996;15:507–525. [PubMed: 9034607]
12. Gilles C, Polette M, Zahm J, et al. Vimentin contributes to human mammary epithelial cell migration. J Cell Sci 1999;112:4615–4625. [PubMed: 10574710]
13. McInroy L, Maata A. Down-regulation of vimentin expression inhibits carcinoma cell migration and adhesion. Biochem Biophys Res Commun 2007;360:109–114. [PubMed: 17585878]
14. Paccione RJ, Miyazaki H, Patel V, et al. Keratin downregulation in vimentin-positive cancer cells is reversible by vimentin RNAi, which inhibits growth and motility. Mol Cancer Ther 2008;7:2898–2903.
15. Schmeichel KL, Bissell MJ. Modeling tissue-specific signaling and organ function in three dimensions. J Cell Sci 2003;116:2377–2388. [PubMed: 12766184]

16. Kleinman HK, McGarvey ML, Hassell JR, et al. Basement membrane complexes with biological activity. Biochemistry 1986;25:312–318. [PubMed: 2937447]
17. Streuli CH, Bissell MJ. Expression of extracellular matrix components is regulated by substratum. J Cell Biol 1990;110:1405–1415. [PubMed: 2182652]
18. Bello-DeOcampo D, Kleinman HK, Deocampo ND, Webber MM. Laminin-1 and alpha 6 beta 1 integrin regulate acinar morphogenesis of normal and malignant human prostate epithelial cells. Prostate 2001;46:142–153. [PubMed: 11170142]
19. Lang SH, Sharrard RM, Stark M, Villette JM, Maitland NJ. Prostate epithelial cell lines form spheroids with evidence of glandular differentiation in three-dimensional Matrigel cultures. Br J Cancer 2001;85:590–599. [PubMed: 11506501]
20. Bae VL, Jackson-Cook CK, Brothman AR, Maygarden SJ, Ware JL. Tumorigenicity of SV40 T antigen immortalized human prostate epithelial cells: association with decreased epidermal growth factor receptor (EGFR) expression. Int J Cancer 1994;58:721–729. [PubMed: 8077059]
21. Bae VL, Jackson-Cook CK, Maygarden SJ, Plymate SR, Chen J, Ware JL. Metastatic sublines of an SV40 large T antigen immortalized human prostate epithelial cell line. Prostate 1998;34:275–282. [PubMed: 9496902]
22. Astbury C, Jackson-Cook CK, Culp SH, Paisley TE, Ware JL. Suppression of tumorigenicity in the human prostate cancer cell line M12 via microcell-mediated restoration of chromosome 19. Genes, Chromosomes Cancer 2001;31:143–155. [PubMed: 11319802]
23. Lee GY, Kenny PA, Lee EH, Bissell MJ. Three-dimensional culture models of normal and malignant breast epithelial cells. Nat Methods 2007;4:359–365. [PubMed: 17396127]
24. Liu X, Wu Y, Zehner ZE, Jackson-Cook CK, Ware JL. Proteomic analysis of the tumorigenic human prostate cell line M12 after microcell-mediated transfer of chromosome 19 demonstrates reduction of vimentin. Electrophoresis 2003;24:3445–3453. [PubMed: 14595690]
25. Hagan M, Yacoub A, Dent P. Ionizing radiation causes a dose-dependent release of transforming growth factor alpha in vitro from irradiated xenografts and during palliative treatment of hormone-refractory prostate carcinoma. Clin Cancer Res 2004;10:5724–5731. [PubMed: 15355899]
26. Zhang X, Diab IH, Zehner ZE. ZBP-89 represses vimentin gene transcription by interacting with the transcriptional activator, Sp1. Nucl Acids Res 2003;31:2900–2914. [PubMed: 12771217]
27. Herrmann ME, Trevor KT. Epithelial-mesenchymal transition during cell culture of primary thyroid tumors? Genes Chromosomes Cancer 1993;6:239–243. [PubMed: 7685628]
28. Thompson EW, Paik S, Brunner N, et al. Association of increased basement membrane invasiveness with absence of estrogen receptor and expression of vimentin in human breast cancer cell lines. J Cell Physiol 1992;150:534–544. [PubMed: 1537883]
29. Hendrix MJ, Seftor EA, Seftor RE, Trevor KT. Experimental co-expression of vimentin and keratin intermediate filaments in human breast cancer cells results in phenotypic interconversion and increased invasive behavior. Am J Path 1997;150:483–495. [PubMed: 9033265]
30. Nagle RB, Hao J, Knox JD, Dalkin BL, Clark V, Cress AE. Expression of hemidesmosomal and extracellular matrix proteins by normal and malignant human prostate tissue. Am J Pathol 1995;146:1498–1507. [PubMed: 7778688]
31. Plymate SR, Tennant MK, Culp SH, et al. Androgen Receptor (AR) expression in AR-negative prostate cancer cells results in differential effects of DHT and IFG-I on proliferation and AR activity between localized and metastatic tumors. Prostate 2004;61:276–290. [PubMed: 15368471]
32. vanLeenders G, Gage WR, Hicks JL, et al. Intermediate cells in human prostate epithelium are enriched in proliferative inflammatory atrophy. Am J Pathol 2003;162:1529–1537. [PubMed: 12707036]
33. vanLeenders GJ, Aalders TW, Hulsbergen-van de Kaa CA, Ruiter DJ, Schalken JA. Expression of basal cell keratins in human prostate cancer metastases and cell lines. J Pathol 2001;195:563–570. [PubMed: 11745692]
34. Abrahams NA, Bostwick DG, Ormsby AH, Qian J, Brainard JA. Distinguishing atrophy and high-grade prostatic intraepithelial neoplasia from prostatic adeno-carcinoma with and without previous adjuvant hormone therapy with the aid of cytokeratin 5/6. Am J Clin Pathol 2003;120:368–376. [PubMed: 14502799]

35. Klezovitch O, Risk M, Coleman I, et al. A causal role for ERG in neoplastic transformation of prostate epithelium. Proc Natl Acad Sci U S A 2008;105:2105–2110. [PubMed: 18245377]
36. Bello-DeOcampo D, Kleinman HK, Webber MM. The role of alpha 6 beta 1 integrin and EGF in normal and malignant acinar morphogenesis of human prostatic epithelial cells. Mutat Res 2001;480–481:209–217.
37. Wu M, Bai X, Xu G, et al. Proteome analysis of human androgen-independent prostate cancer cell lines: variable metastatic potentials correlated with vimentin expression. Proteomics 2007;7:1973–1983. [PubMed: 17566973]
38. Eckes B, Dogic D, Colucci-Guyon E, et al. Impaired mechanical stability, migration and contractile capacity in vimentin-deficient fibroblasts. J Cell Sci 1998;111:1897–1907. [PubMed: 9625752]
39. Singh S, Sadacharan S, Su S, Belldegrun A, Persad S, Singh G. Overexpression of vimentin: role in the invasive phenotype in an androgen-independent model of prostate cancer. Cancer Res 2003;63:2306–2311. [PubMed: 12727854]
40. Weaver VM, Petersen OW, Wang F, et al. Reversion of the malignant phenotype of human breast cells in three-dimensional culture and in vivo by integrin blocking antibodies. J Cell Biol 1997;137:231–245. [PubMed: 9105051]
41. Park C, Zhang H, Pallavicini M, et al. Beta 1 integrin inhibitory antibody induces apoptosis of breast cancer cells, inhibits growth, and distinguishes malignant from normal phenotype in 3D cultures and *in vivo*. Cancer Res 2006;66:1526–1535. [PubMed: 16452209]
42. Ivaska J, Vuoriluoto K, Huovinen T, Izawa I, Inagaki M, Parker PJ. PKCε-mediated phosphorylation of vimentin controls integrin recycling and motility. EMBO J 2005;24:3834–3845. [PubMed: 16270034]
43. Helfand BT, Chang L, Goldman RD. Intermediate filaments are dynamic and motile elements of cellular architecture. J Cell Sci 2004;117:133–141. [PubMed: 14676269]
44. Helfand BT, Chou Y-H, Shumaker DK, Goldman RD. Intermediate filament proteins participate in signal transduction. Trends Cell Biol 2005;15:568–570. [PubMed: 16213139]
45. Rabinovitz I, Nagle RB, Cress AE. Integrin alpha 6 expression in human prostate carcinoma cells is associated with a migratory and invasive phenotype in vitro and in vivo. Clin Exp Metastasis 1995;13:481–491. [PubMed: 7586806]
46. Edlund M, Miyamoto T, Sikes RA, et al. Integrin expression and usage by prostate cancer cell lines on laminin substrata. Cell Growth Differ 2001;12:99–107. [PubMed: 11243469]
47. Lang SH, Hyde C, Reid IN, Hitchcock IS, Hart CA, Bryden AA, Villette JM, Stower MJ, Maitland NJ. Enhanced expression of vimentin in motile prostate cell lines and in poorly differentiated and metastatic prostate carcinoma. Prostate 2002;52:253–263. [PubMed: 12210485]

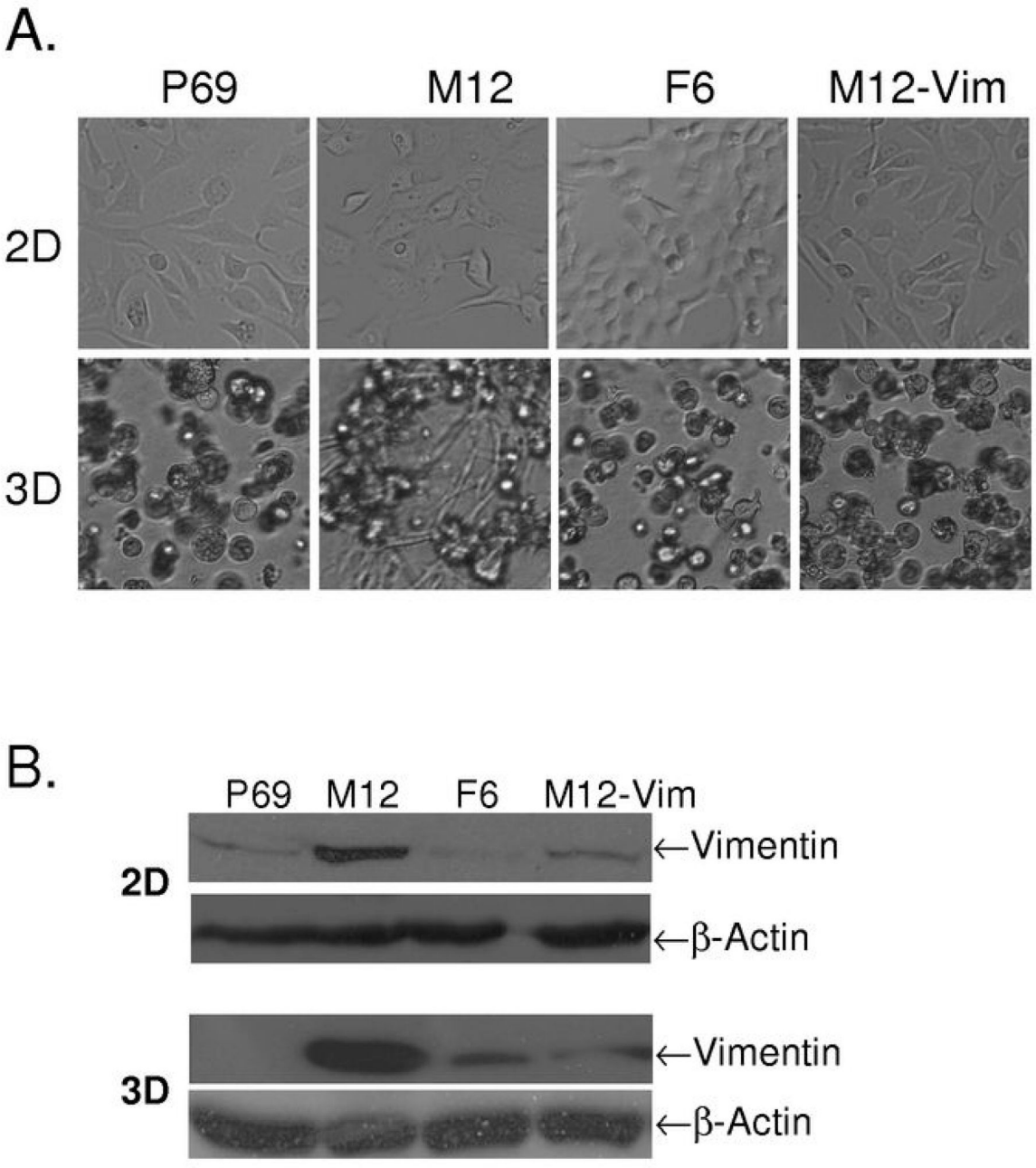

Fig. 1.

Comparison of the morphology of P69, M12, F6 and M12-Vim prostate sublines grown on tissue culture dishes (2D) versus embedded in lrECM gels (3D). **(A)** Light microscopy images of these various prostate cancer sublines were taken from cultures grown in 2D on traditional plastic dishes for 4 days versus 8 days embedded in lrECM (3D) as described in Materials and Methods. Magnification is at 10X. **(B)** Whole cell extracts (40 μg) from 2D and 3D cultures of these sublines were subjected to Western blot analysis with vimentin antibody as described in Materials and Methods. β-actin was used as loading control.

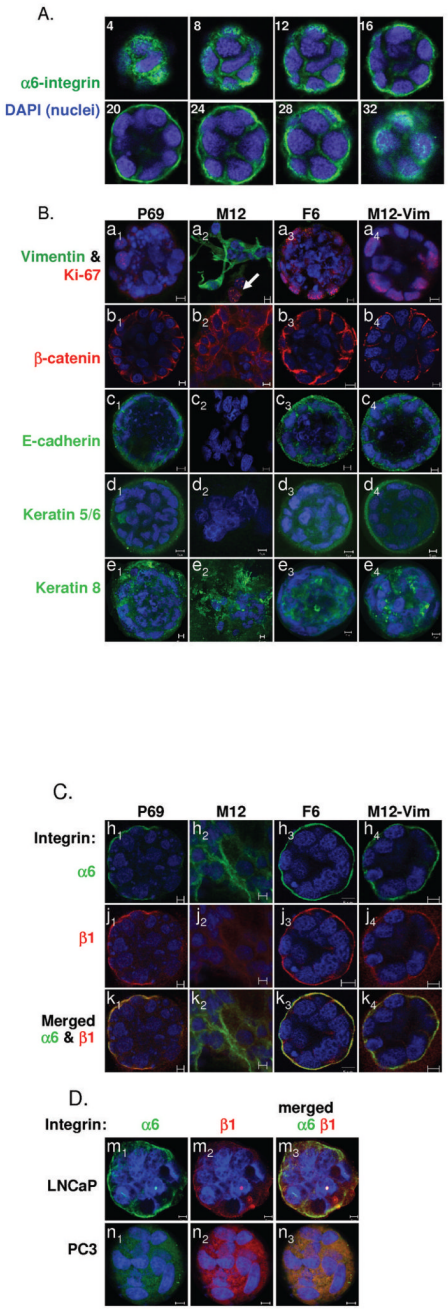

Fig. 2.

Comparison of content and localization of relevant proteins within the various morphological structures formed by the P69, M12, F6 and M12-Vim prostate sublines grown embedded in lrECM gels. (**A)** A Z-stack of P69 acini from day 8 3D cultures was examined by immunofluorescence confocal microscopy. These 8 pictures represent plane 4, 8, 12, 16, 20, 24, 28 and 32 from 40 such planes. Acini were fixed and stained with antibody to α6-integrin (green). All pictures are taken at a magnification of 63X and nuclei were counterstained with DAPI (blue) as discussed in Materials and Methods. **(B)** Confocal immunofluorescence microscopy of structures formed by the various sublines at day 8 in lrECM stained with antibodies to vimentin (green) and Ki-67 (red), panels a_1 to a_4; β-catenin (red), panels b_1 to

b_4; and E-cadherin (green), panels c_1 to c_4; keratin 5/6 (green), panels d_1 to d_4; keratin 8 (green), panels e_1 to e_4; and nuclei (blue) in all panels. **(C)** Cellular structures were stained with antibodies to α6-integrin (green), panels h_1 to h_4, or β1-integrin (red), panels j_1 to j_4 with overlay of α6β4 integrin in panel k_4. For details of immunostaining see Materials and Methods. (**D**) LnCap and PC3 cell lines were grown in lrECM and stained at day 8 as described in panel C. For panels B, C and D a size marker of 5 μm is shown.

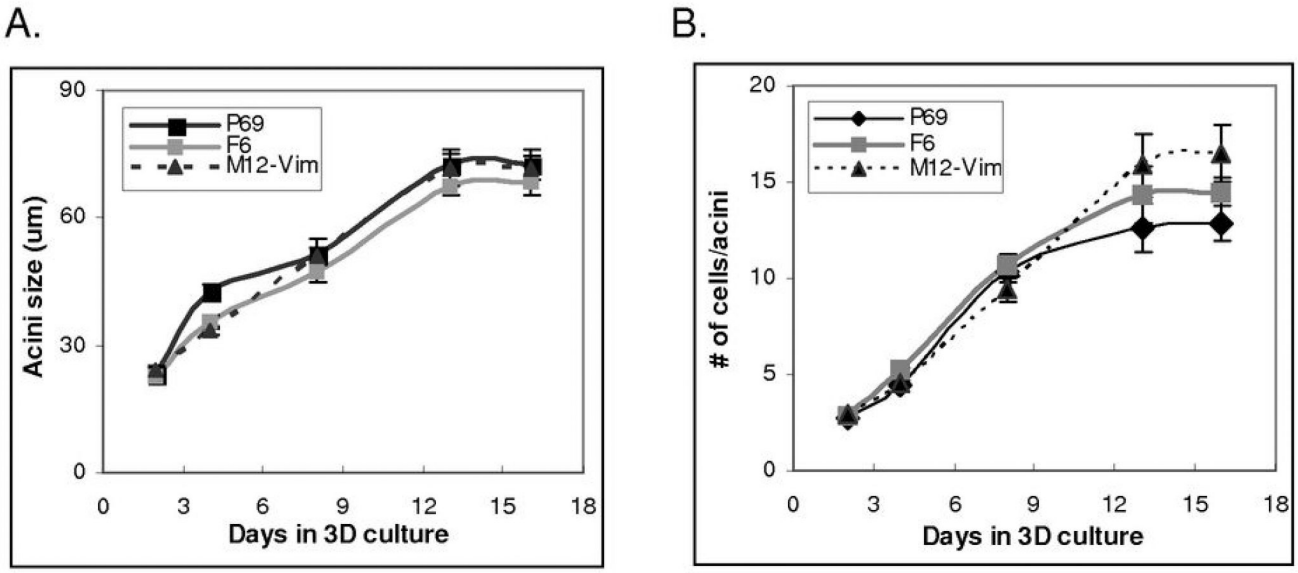

Fig. 3.

Growth properties of P69, F6, and M12-Vim acini in 3D culture. **(A)** Acini were isolated from P69, F6 and M12-Vim cultures grown embedded in lrECM gels for 2, 4, 8, 13 and 16 days. The average cell number per acini cross-section (from at least 100 acini) was counted using confocal microscopy. The standard error of the mean is shown as error bars. **(B)** The average size of (μm) of acini (from at least 25 acini) was measured as in panel A. The standard error of the mean is shown as error bars.

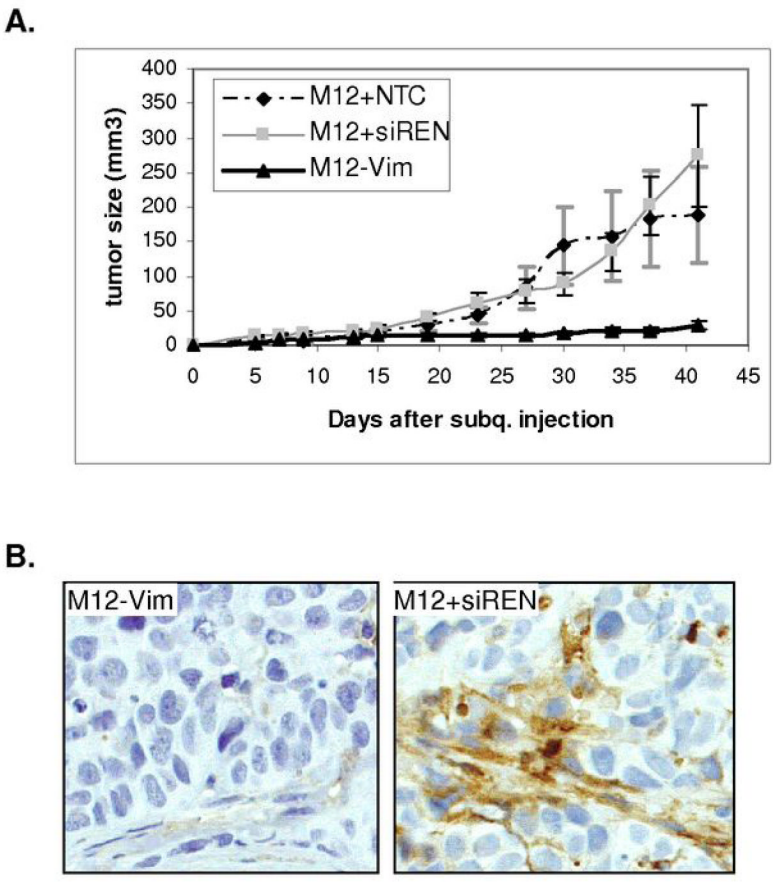

Fig. 4.

Tumorigenic properties of M12-Vim cells are reduced in athymic mice. (**A)** Tumor formation following subcutaneous injection of 1×10^6 M12-Vim cells (6 mice) was compared to the injection of cells containing vector only M12+siREN (4 mice) or M12+NTC, a non-targeting RNA control, (5 mice). Tumor growth was monitored by caliber measurement each 4 to 5 days for up to 42 days. All animals displayed tumors albeit of varying size and tumor volume (mm^3), calculated as described in Materials and Methods. The standard error of the mean is shown as error bars. **(B)** immunofluoresence staining with human vimentin antibody of paraffin-embedded M12+siREN (left panel) and M12-Vim (right panel) tumors retrieved from nude mice at time of euthanasia (42 days). Magnification is at 400X.

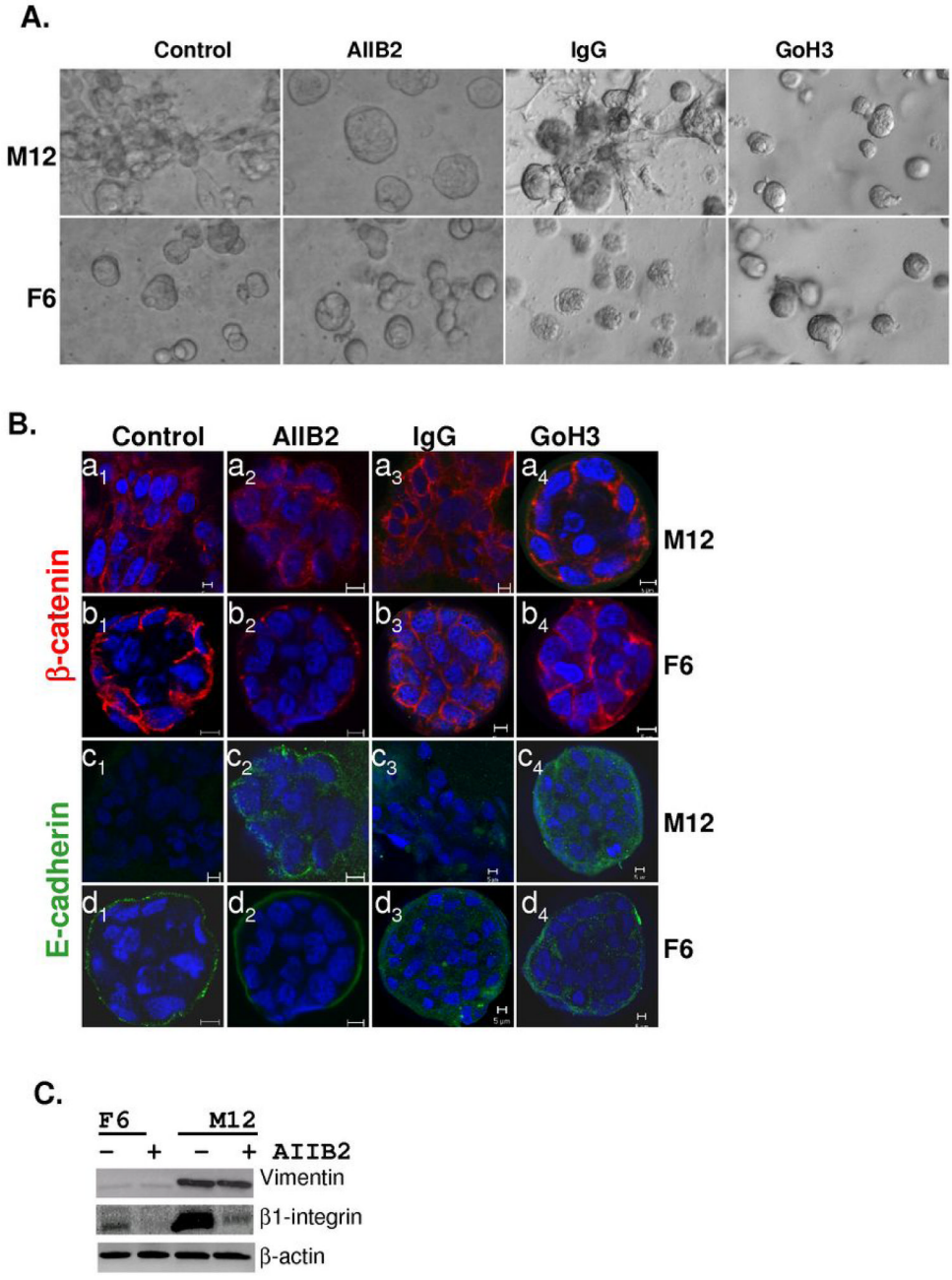

Fig. 5.

Inclusion of blocking antibodies to β1-integrin (AIIB2) or α6-integrin (GoH3) leads to the formation of reverted acini with the metastatic M12 subline. **(A)** Light microscopy images of the M12 and F6 subline grown embedded in lrECM for 10 days in the absence or presence of inhibitory antibodies or IgG as a negative control are noted. Magnification is at 20X. **(B)** Confocal immunofluorescence microscopy of the M12 or F6 subline grown embedded in lrECM for 10 days in the absence or presence of AIIB2, GoH3 or IgG as indicated. Cells were stained with E-cadherin (green) and β-catenin (red) and nuclei were stained with DAPI (blue). Magnification is at 63X and a size marker of 5 μm is shown. **(C)** Whole cell extracts (40 μg)

from 10 day cultures as described in panel A were subjected to Western blot analysis with vimentin, β1-integrin, or β-actin antibody.

Table 1

Summary of the *in vivo* and *in vitro* Properties of the Prostate Cancer Sublines

69	M12
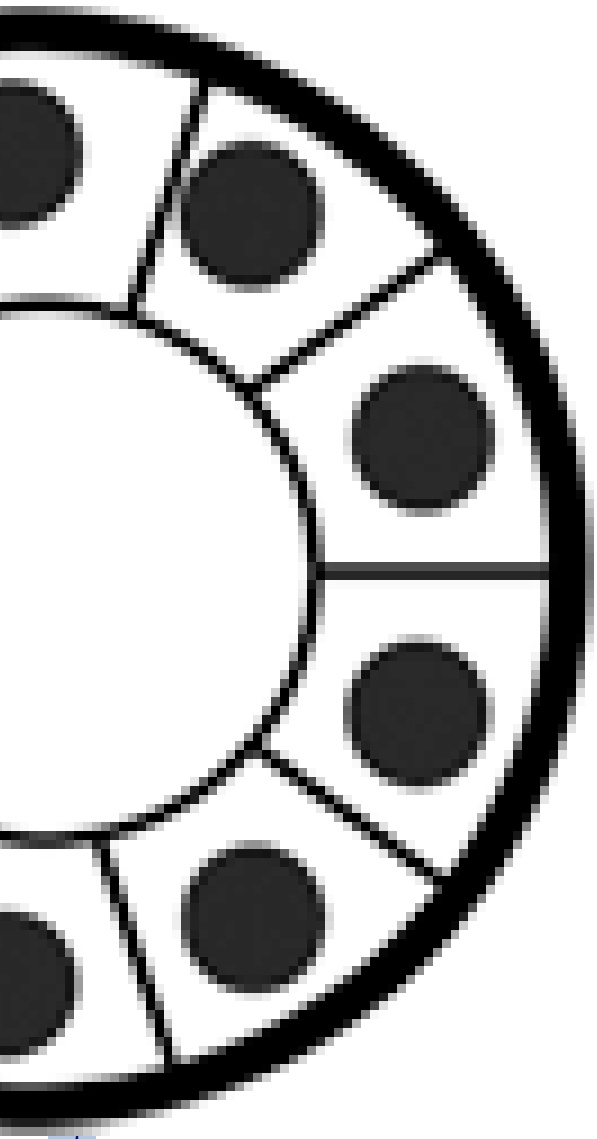	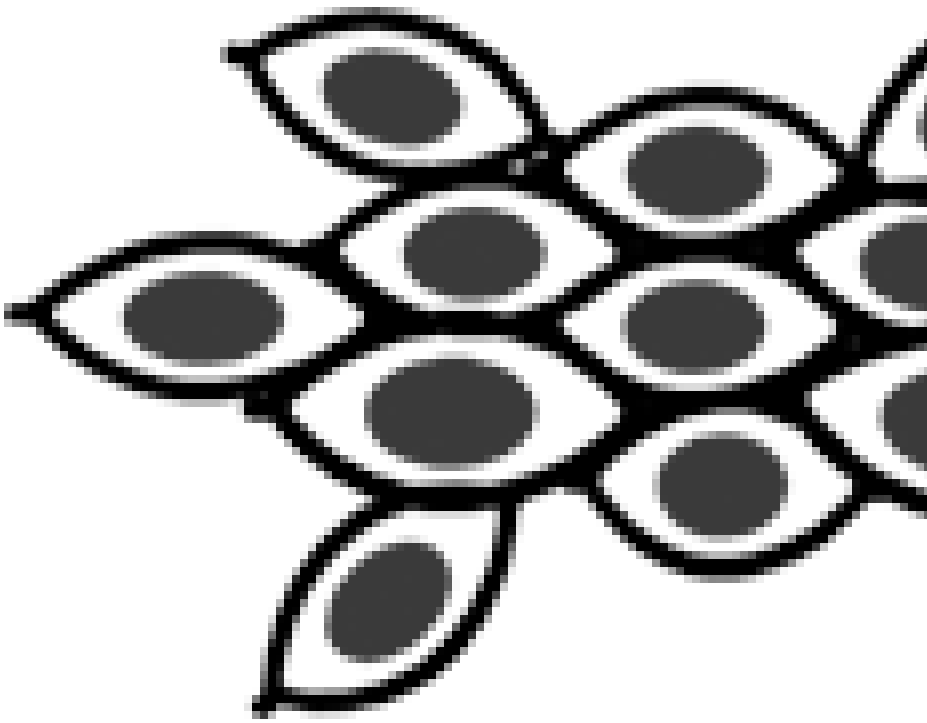
Non	Yes
Yes	No
+++	–
–	+++
+++	–

69	M12
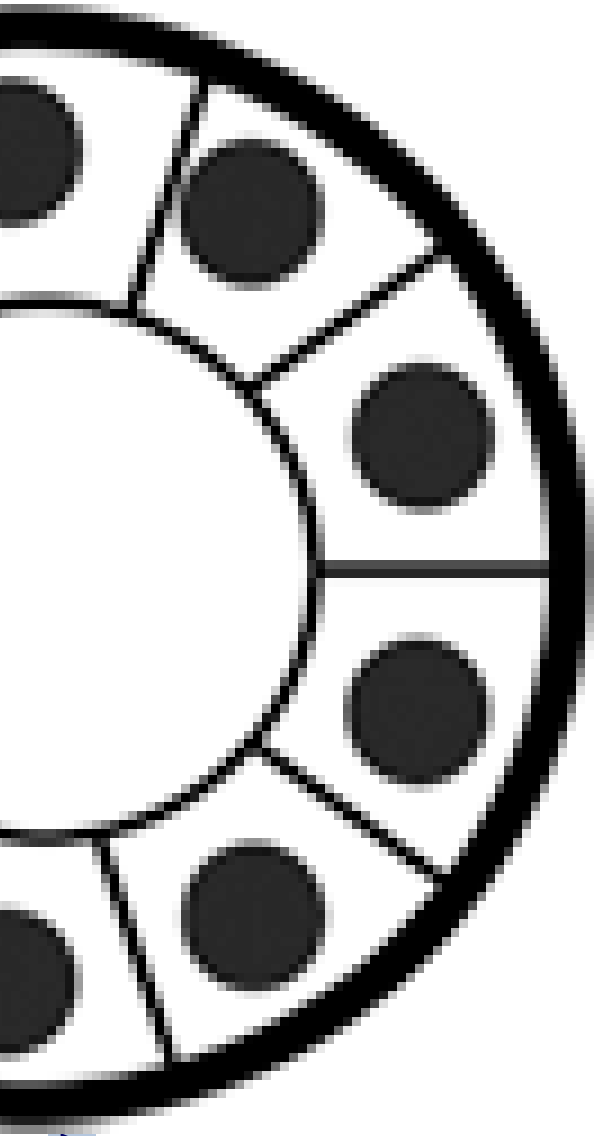	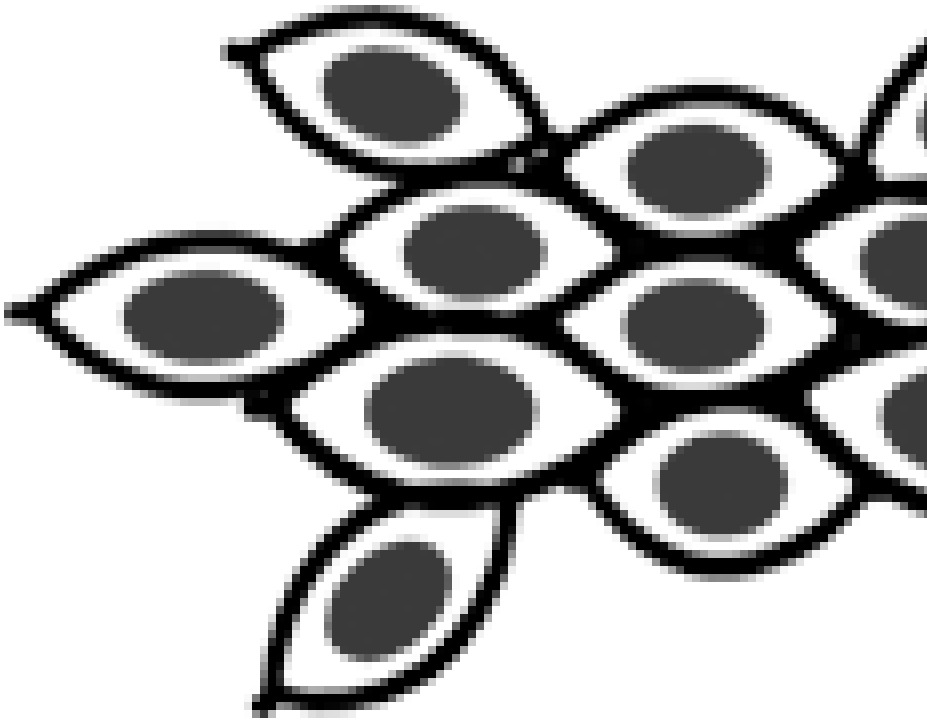
+++	+++
+++	+++
al Polarity	Non-Polarized
al Polarity	Non-Polarized